PERGAMON

Micron 33 (2002) 385–397

micron

www.elsevier.com/locate/micron

Review

Imaging and manipulation of biological structures with the AFM

Dimitrios Fotiadis[a], Simon Scheuring[a], Shirley A. Müller[a], Andreas Engel[a], Daniel J. Müller[a,b,*]

[a]*M. E. Müller Institute for Microscopy, Biozentrum of the University of Basel, CH-4056 Basel, Switzerland*
[b]*Max-Planck-Institute of Molecular Cell Biology and Genetics, D-01307 Dresden, Germany*

Received 15 February 2001; revised 28 April 2001

Abstract

Many biologists have dreamt of physically touching and manipulating the biomolecules they were investigating. With the invention of the atomic force microscope (AFM), this dream has come true. Here, recent applications of the AFM to image and to manipulate biological systems at the nanometer scale are reviewed. Macromolecular biological assemblies as well as individual biomolecules can be subjected to controlled nanomanipulation. Examples of AFM application in imaging and nanomanipulation include the extraction of chromosomal DNA for genetic analysis, the disruption of antibody–antigen bonds, the dissection of biological membranes, the nanodissection of protein complexes, and the controlled modulation of protein conformations. Also reviewed is the novel combination of single molecule imaging and force spectroscopy which allows biomolecules to be imaged, and inter- and intramolecular forces to be measured. Future application of these nanotechniques will reveal new information on the structure, function and assembly of biomolecules.

Keywords: Atomic force microscopy; Force spectroscopy; Nanodissection; Nanomanipulation; Single molecule imaging

Contents

1. Introduction

Understanding how complexes of biomolecules are assembled is of fundamental importance to elucidate their structure and function. To gain new insights into these supramolecular assemblies, techniques are required that provide information at the level of single molecules (Science, 1999; Nature Structural Biology, 2000). Among these, the atomic force microscope (AFM) is unique since it not only allows individual molecules to be imaged (Shao and Yang, 1995; Czajkowsky and Shao, 1998; Engel and Müller, 2000) but also to be manipulated (Clausen-Schaumann et al., 2000; Fisher et al., 2000; Rief et al., 2000).

Since the invention of the AFM (Binnig et al., 1986) amazing progress has been made in the imaging of biomolecules. This progress is due to the combined efforts of

* Corresponding author. Tel.: +49-351-2102586; fax: +49-351-2101209.
E-mail address: daniel.mueller@mpi-cbg.de (D.J. Müller).

Abbreviations: 2D, Two-dimensional; AFM, Atomic force microscope; BR, Bacteriorhodopsin; CM, Contact mode; HPI, Hexagonally packed intermediate; MIP, Major intrinsic protein; PSI, Photosystem I; S-layer, Surface-layer; TM, Tapping mode

0968–4328/02/$ - see front matter
PII: S0968-4328(01)00026-9

numerous laboratories to improve instrumentation (Hansma et al., 1994; Putman et al., 1994; Viani et al., 1999; Humphris et al., 2000), AFM probes (Walters et al., 1996; Cheung et al., 2000; Schmitt et al., 2000), sample preparation methods (Müller et al., 1997a; Wagner, 1998), and image acquisition conditions (Müller et al., 1999b). The AFM has several unique features that are very useful for biological studies: Firstly, it can be operated in solution allowing biological structures to be observed in their native environment (Drake et al., 1989). Secondly, the AFM provides such a high signal-to-noise ratio that single proteins can be observed at a resolution better than 1 nm (Mou et al., 1995; Müller et al., 1995b; Walz et al., 1996; Czajkowsky et al., 1998; Reviakine et al., 1998; Scheuring et al., 1999; Fotiadis et al., 2000). Thirdly, conformational changes of single biomolecules can be directly visualized (Müller et al., 1995a, 1996a; Müller and Engel, 1999). In fact single biomolecules can now be observed at work (Kasas et al., 1997; Grandbois et al., 1998; Viani et al., 2000) for a review see (Engel and Müller, 2000).

Furthermore, the past few years have demonstrated that the combination of AFM imaging and manipulation, allows the precise and controlled modification of biological systems from the level of the cell down to the scale of individual molecules (Schoenenberger and Hoh, 1994; Thalhammer et al., 1997; Fotiadis et al., 1998). In this review the unique possibilities provided by the AFM are presented and the novel information thereby obtained is discussed.

2. Principles of AFM imaging

The principle of the AFM is relatively simple: A sharp probe (tip) mounted at the end of a flexible cantilever raster-scans over the sample surface in a series of horizontal sweeps (Binnig et al., 1986). Deflections of the cantilever caused by the probe-sample interaction are detected by an optical detector (Meyer and Amer, 1988; Alexander et al., 1989). This signal is used to minimize the force applied to the sample by moving the sample up and down via a servo-system. The surface topography is then reconstructed from the vertical movements of the sample which are driven by a computer-controlled piezo. In this imaging mode, called contact mode (CM), the probe is always in contact with the sample.

The AFM cannot only operate in air or in high vacuum, but also in liquids. Imaging in aqueous solution permits the observation of biomolecules under physiological conditions and eliminates the strong capillary forces occurring between probe and sample when imaging is performed in air (Weisenhorn et al., 1989). This breakthrough, key for the application of the AFM in biology, came with the development of the fluid cell (Drake et al., 1989). To prevent deformation of the soft biological sample by the probe, the vertical force applied to the AFM cantilever is typically adjusted to 50–100 pN (minimum force). At applied forces between 100 and 1000 pN the biological specimen is deformed reversibly (Müller et al., 1995a,b; Scheuring et al., 1999; Heymann et al., 2000). At forces above these values, the sample may be deformed irreversibly. The interplay between applied force and deformation of the specimen is most easily observed by comparing the surface topographs of the biological samples before and after applying enhanced forces.

To manipulate biomolecules, the applied force has to be controlled in a precise manner while other forces, such as frictional forces, have to be reduced to a negligable amount. In CM–AFM, these forces can be reduced significantly by damping interactions between the biological molecules and the AFM probe electrostatically (Müller et al., 1999b). Here, the electrostatic double layer repulsion compensates most of the applied force and distributes this force over a large surface area of the sample. After careful adjustment of the electrolyte concentration and pH of the imaging buffer, the effective force that remains interacting locally on molecular structures is sufficiently small to allow the unperturbed structure of biological macromolecules to be imaged at a lateral resolution of ~0.5 nm and a vertical resolution of ~0.1 nm. Although this is an efficient technique, it requires a series of experiments for each protein examined to ensure that the optimal electrostatic balance is obtained. An alternative approach is to reduce the frictional forces produced as the tip moves across the sample. This has resulted in the development of two alternative AFM modes, the tapping mode (TM) (Zhong et al., 1993; Hansma et al., 1994; Putman et al., 1994) and the magnetically activated oscillating mode (MAC) (Han et al., 1996, 1997). Both are frequently used and have in common that the AFM cantilever is oscillated vertically while scanning the object. When the imaging parameters are adjusted correctly, the probe touches the sample very briefly at the end of its downward movement (Tamayo and Garcia, 1996). Because these imaging modes reduce the frictional forces, they can be used to image single biomolecules that are only weakly immobilized on a support, whereas CM–AFM has the tendency to sweep away corrugated and weakly immobilized objects. However, the spatial resolution currently achieved by TM- and MAC–AFM is lower than that achieved by CM–AFM (Möller et al., 1999; compare: Mou et al., 1996; Cheung et al., 2000; Viani et al., 2000).

3. Imaging and dissection of isolated DNA and human metaphase chromosomes

The first controlled nanomanipulation of biomolecules using the AFM was performed on genetic material (Hansma et al., 1992). Isolated DNA adsorbed to a mica surface was dissected, both in air (Henderson, 1992; Vesenka et al., 1992) and in propanol (Hansma et al., 1992) by increasing the force applied to the AFM probe to about 5 nN. This demonstrated for the first time the feasibility of dissections in the nanometer range.

In the nucleus of eukaryotic cells, DNA is packaged with

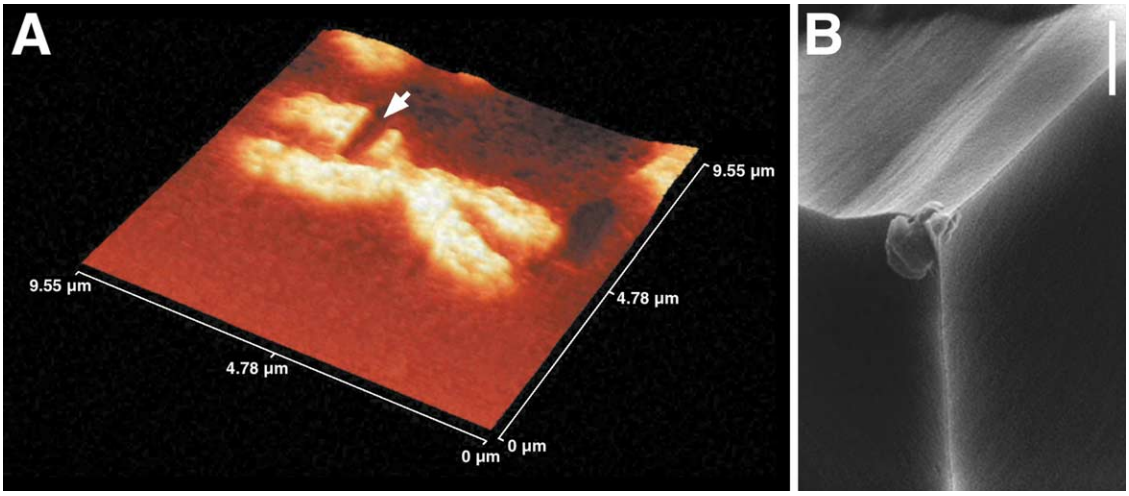

Fig. 1. DNA extraction of human chromosome 2. (A) AFM topograph of human chromosome 2 recorded after dissection. The DNA dissection and extraction site is marked by an arrow. The topograph was recorded in air using tapping mode AFM. The DNA extraction was performed in the contact mode. The topograph exhibits a vertical brightness range of 190 nm and is displayed as a relief. (B), Scanning electron microscopy image of the AFM probe after DNA extraction. Biological material from the dissected chromosome can clearly be seen adhering to the probe apex. The scale bar in B represents 1 μm.

proteins to form chromatin which is further condensed to chromosomes, visible during metaphase as distinct morphological entities. AFM topographs of plant (Winfield et al., 1995; McMaster et al., 1996b), insect (Mosher et al., 1994; Jondle et al., 1995; Vesenka et al., 1995), and human (de Grooth and Putman, 1992; Rasch et al., 1993; Fritzsche et al., 1994) chromosomes with nanometer lateral resolution and subnanometer vertical resolution have been acquired by various groups. In addition, volumes calculated from AFM topographs have allowed chromosomes to be classified (karyotyped) (Fritzsche and Henderson, 1996; McMaster et al., 1996a). Besides for imaging, the AFM can be used to precisely dissect and subsequently extract genetic material from chromosomes (Thalhammer et al., 1997; Xu and Ikai, 1998). As illustrated in Fig. 1A, chromosomes can be dissected at selected locations and these can be precisely documented (Thalhammer et al., 1997; Stark et al., 1998). In the experiments made, at loading forces of applied $F > 17$ μN tip to the genetic material removed by dissection adhered to the AFM probe (Fig. 1B). The extracted DNA was amplified by polymerase chain reaction (PCR) and finally used to assess the specificity of the procedure by fluorescence in situ hybridization (FISH) (Thalhammer et al., 1997). In the future, AFM combined with fluorescence microscopy, PCR and FISH may play an important role in cytogenetic studies, such as the generation of chromosome band-specific libraries and high-resolution physical mapping of genomes.

4. Disruption of antibody and antigen bonds

Immunolabelling and other labelling techniques are nowadays well established and used routinely in light and electron microscopy. They provide biologists with a wealth of information at both the cellular and the molecular levels. Recently, labelling techniques have found an application in combined light and atomic force microscopy (Putman et al., 1993; Schabert et al., 1994; Hillner et al., 1995). The use of these two complementary microscopy techniques in parallel, for example to examine cells, allows the position of structures labeled with fluorescent markers to be determined while the cellular surface is imaged under physiological conditions (for reviews see: Vesenka et al., 1995; Schoenenberger et al., 1997). However, in most cases the biological specimen has been chemically fixed before labelling and thus, the AFM is no longer imaging the native structure.

An alternative approach employs antibody labelling to determine the sidedness of native membrane protein surfaces in a physiological environment by AFM. At low magnification, individual purple membrane patches adsorbed to mica are indistinguishable, whereas two distinct surface topographies become apparent at submolecular resolution (Müller et al., 1995b, 1999c). This indicates that both, the cytoplasmic and the extracellular surfaces of bacteriorhodopsin (BR) trimers, were imaged. To identify the sidedness, purple membrane patches adsorbed to mica were incubated with antibodies directed against the cytoplasmic C-terminus of BR and subsequently imaged in their presence without fixation. As a result of antibody binding, a number of membrane patches displayed a heavily textured surface (Fig. 2A) whereas other membrane surfaces (extracellular) were unaffected by the presence of antibodies (Müller et al., 1996b). The antibodies that had specifically bound to the cytoplasmic membrane surface could be displaced at applied forces of >0.8 nN (Fig. 2B). Images of the unveiled surface topography at molecular resolution (Fig. 2C) identified the donut-shaped BR trimers as the cytoplasmic side of the purple membrane (Müller et al., 1996b; Heymann et al., 1999). When the AFM probe was

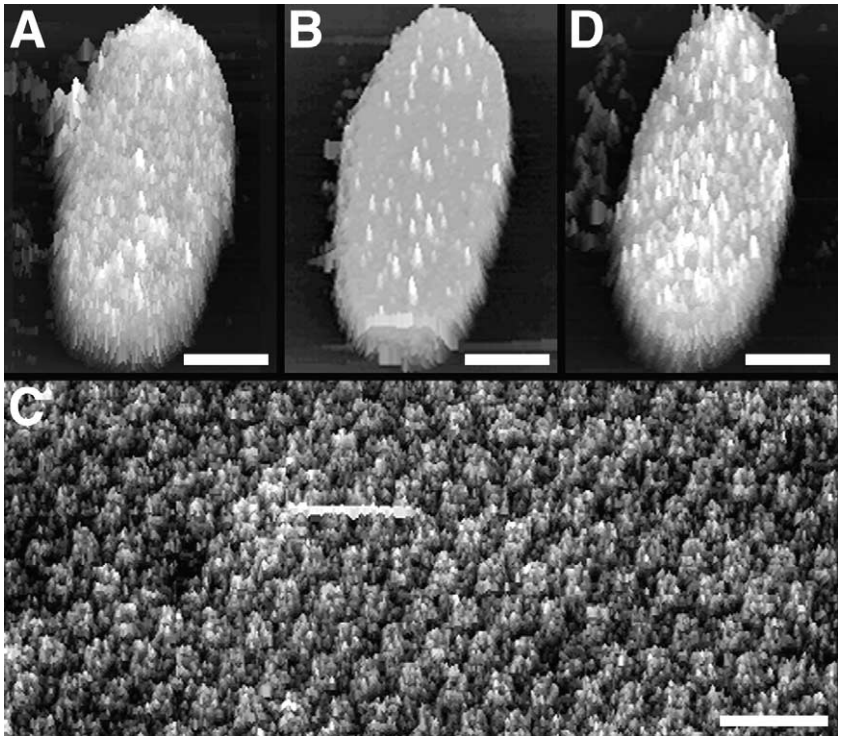

Fig. 2. Disruption of antibody-antigen bonds by AFM to determine the sidedness of bacteriorhodopsin. (A) Purple membrane from *Halobacterium salinarum* densely labeled with antibodies against the C-terminus which is situated on the cytoplasmic side of BR. (B) Increasing the force applied to the AFM cantilever to >0.8 nN resulted in the mechanical removal of the antibodies from the cytoplasmic BR surface. (C) Removal of the antibodies unveiled the characteristic structure of the cytoplasmic purple membrane surface. (D) Relabelling of the purple membrane by antibodies present in the buffer solution occurred if the AFM probe was withdrawn for some minutes. The contact mode topographs were recorded in buffer solution (150 mM KCl, 10 mM Tris–HCl, pH 9.2). Scale bars represent 200 nm (A, B, and D) and 15 nm (C). The topographs exhibit vertical brightness ranges of 25 nm (A, B, and D) and 1 nm (C) and are displayed as reliefs tilted by 5°.

withdrawn for a few minutes, the cytoplasmic surface regions, previously cleared from antibodies, were relabeled by the free antibodies present in the imaging buffer (Fig. 2D).

5. Nanodissection of membranes

Cell-to-cell interactions involve the adhesion of two cell membranes to one another. This is mediated by the extracellular regions of specific membrane proteins. When isolated and reconstituted, such membrane proteins also interact via their extracellular surfaces giving rise to 'sandwiched' structures. Examples are the extracellular surfaces of gap junction connexins (Hoh et al., 1993), porin OmpF from *Escherichia coli* (Schabert et al., 1995) and the major intrinsic protein (MIP) from sheep eye lenses (Fotiadis et al., 2000). While the functional and structural importance of the extracellular interaction of connexins (Perkins et al., 1998; Unger et al., 1999) and MIPs (Benedetti et al., 2000; Fotiadis et al., 2000) have been elucidated, it is at present not clear whether the porin–porin adhesion is related to a biological function. Atomic force microscopy is nowadays well established as a technique to examine the native surface structure of membrane proteins incorporated in a lipid bilayer (Shao and Yang, 1995; Engel et al., 1997). However, sandwiched membrane proteins pose a problem since the extracellular surfaces must be uncovered to make them accessible to the AFM probe.

In situ, gap junctions consist of two stacked plasma membranes. The individual connexons of opposite membranes are in register and thus form a channel (Unwin and Ennis, 1984) between adjacent cells (Sosinsky, 1996; Perkins et al., 1997). When isolated gap junctions are imaged by AFM, the extracellular surfaces of the connexons are sandwiched between the two membranes, while the cytoplasmic surface is exposed to the AFM probe (Hoh et al., 1991, 1993). Subsequently, the upper membrane of the gap junction can be dislodged by increasing the force applied to the AFM cantilever. This mechanical removal by the AFM tip exposes the extracellular surface of the underlying membrane allowing its structure to be investigated.

Similarly, it has also been possible to dissect double-layered membranes of reconstituted OmpF porin from *Escherichia coli*. In these experiments, the periplasmic surface of OmpF was exposed whereas the extracellular surface was sandwiched. Mechanical removal of the upper membrane by the AFM tip unveiled the extracellular OmpF surface allowing its structural analysis (Schabert and Engel, 1994; Schabert et al., 1995).

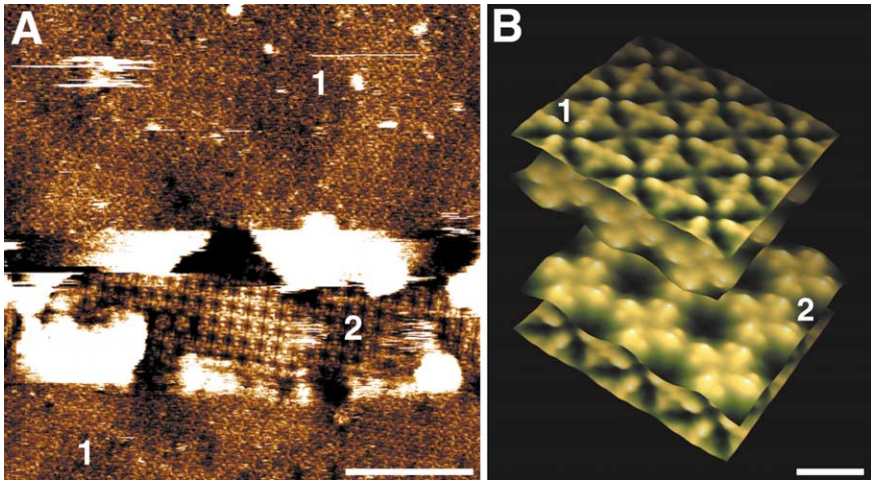

Fig. 3. Structure and interaction mechanisms of stacked 2D MIP crystals. (A) Double-layered MIP crystal imaged after partial removal of the upper layer by the AFM probe. Both, the cytoplasmic and the extracellular surface of MIP are visible. The contact mode topograph was recorded in buffer solution (150 mM KCl, 50 mM $MgCl_2$, 10 mM Tris–HCl, pH 8.8). (B) Computer reconstruction of a double-layered MIP crystal showing the interaction of the extracellular surfaces and the in-register alignment of the two crystalline sheets. The cytoplasmic surface of MIP (1) is characterized by a weak corrugation which is absent on the extracellular surface (2). Scale bars represent 50 nm (A) and 5 nm (B). The topographs exhibit vertical brightness ranges of 1.8 nm (A) and 1.4 nm (B).

The widely spread disease cataract results from disruption (Shiels et al., 2000) or mutations (Shiels and Bassnett, 1996) in the gene for MIP. Purified MIP protein from ovine eye lenses reconstituted in the presence of lipids forms highly ordered tetragonal 2D arrays (Hasler et al., 1998) which have the tendency to form double layers. In these sandwiches the extracellular surfaces of the tetrameric proteins interact in a highly specific manner, thereby hiding from the AFM tip (Fotiadis et al., 2000). Increasing the force applied on imaging removes a small fraction of the upper membrane layer and exposes the extracellular surface of MIP from the bottom layer (Fig. 3A). Thus, the

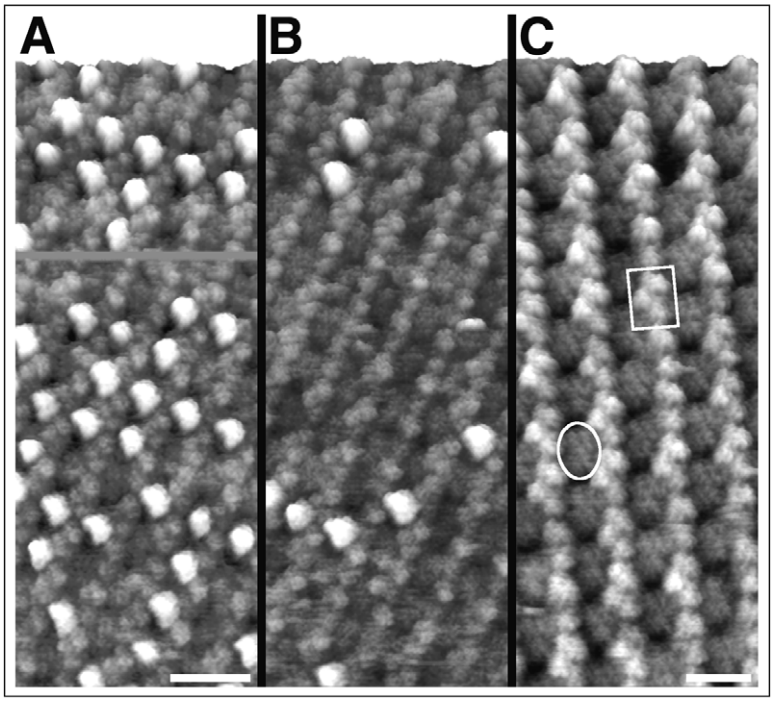

Fig. 4. Dissection of single cyanobacterial photosystem I complexes. (A) Topograph of a 2D PSI crystal. The up-and-down orientation of the PSI complexes which give the crystal a $p12_12$ symmetry is clearly visible. The high protrusions arise from the extrinsic subunits PsaC, PsaD and PsaE located on the stromal side. (B) The water-soluble, extrinsic subunits disappear upon repetitive scanning of the same area. (C) At higher magnification, the stromal surface depleted of the extrinsic subunits unveils the topography of the reaction center core (ellipse). The lumenal surface is marked by a rectangle. Scale bars represent 25 nm (A and B) and 15 nm (C). The contact mode topographs were recorded in buffer solution (300 mM KCl, 20 mM Tris–HCl, pH 7.8), exhibit vertical full gray level ranges of 4 nm (A and B) and 2 nm (C), and are displayed as reliefs tilted by 5°.

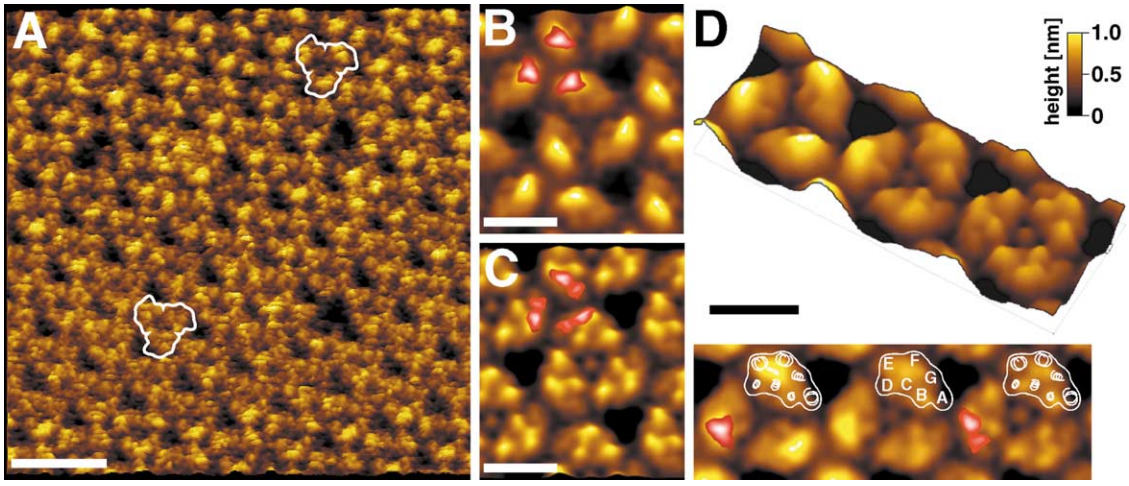

Fig. 5. Mechanical modulation of individual polypeptide loops in bacteriorhodopsin. (A) The cytoplasmic surface topography of purple membrane. At the top of the image the force applied to the AFM probe was 100 pN. While scanning the surface line by line, the force was increased by 100 pN (A, center-bottom region) and then minimized again to 100 pN (A, bottom region). The white contour lines mark BR trimers. The force-induced conformational change of BR is fully reversible (Müller et al., 1995a). Correlation averages of the cytoplasmic BR surface recorded at 100 pN (B) and at 200 pN (C). Surface regions exhibiting a standard deviation above 0.1 nm are depicted in red-to-white shades. D, Interpretation of the force dependent conformational change of BR. Top, perspective view of the transition from low force (100 pN; D, left) to high force BR trimers (200 pN; D, right). The central trimer is a graded overlay of the left trimer recorded at 100 pN and the right trimer recorded at 200 pN. Bottom, corresponding topograph, the helices derived from the atomic model of BR (Grigorieff et al., 1996) are superimposed. The single protrusion evident at low force (D, bottom left) is identified as the loop connecting helices E and F. The individual protrusions evident at high force (200 pN; D, bottom right) represent loops connecting helices A and B, helices C and D, the C-terminal end, and what remains from the compressed EF loop. Surface regions exhibiting a standard deviation above 0.1 nm are depicted in red-to-white shades. The contact mode topograph was recorded in buffer solution (100 mM KCl, 10 mM Tris–HCl, pH 7.8). Scale bars represent 10 nm (A) and 4 nm (B, C and D). The topographs exhibit a vertical brightness range of 1.2 nm (A) and 1.0 nm (B, C and D). A, B and C are displayed as reliefs tilted by 5°.

cytoplasmic (Fig. 3; 1) as well as the extracellular (Fig. 3; 2) MIP surfaces can be visualized. In combination with cryo-electron microscopy data (Fotiadis et al., 2000), such AFM topographs show the extracellular surfaces of interacting MIP tetramers located in opposite membranes to be in precise register (Fig. 3B). These results suggest that in vivo, continuous MIP channels extend from one cell to another and that the precise interaction between the extracellular surfaces contributes to cell-to-cell adhesion and the unique architecture of lens fiber cells in the eye (Fotiadis et al., 2000).

6. Nanodissection of the photosystem I reaction center

The 340 kDa pigment-containing reaction center photosystem I (PSI) from the thermophilic cyanobacterium *Synechococcus* sp. consists of 11 protein subunits (Schubert et al., 1997). Three of these 11 subunits, PsaC, -D and -E, are extrinsic and adhere to the complex via electrostatic interactions (Schubert et al., 1997). Isolated PSI complexes assemble in an up-and-down manner to form 2D crystals in which their lumenal and stromal surfaces are alternately exposed (Karrasch et al., 1996; Fotiadis et al., 1998). When imaged with the AFM, the three extrinsic subunits can be discerned as 3.5 nm high protrusions above the lipid bilayer on the stromal surface (Fig. 4A). Repetitive scanning of such 2D crystals displaces the extrinsic subunits (Fig. 4B) making the underlying surfaces available for structural analysis at high resolution (Fig. 4C) (Fotiadis et al., 1998). Thus, as illustrated by Fig. 4, the AFM tip can be used as a nanoscalpel to remove individual protein subunits allowing the structure of otherwise hidden surfaces to be studied.

7. Modulating polypeptide loops of individual bacteriorhodopsin molecules

On AFM topographs of the cytoplasmic surface, BR exhibits trimeric structures arranged in a trigonal lattice of 6.2 ± 0.2 nm side length (Müller et al., 1995b). At imaging forces of 100 pN, each subunit in the trimer features a pronounced protrusion extending 0.8 ± 0.2 nm above the lipid surface (Fig. 5A, top and Fig. 5B). This protrusion is thought to arise from the loop connecting the α-helices E and F (Müller et al., 1995a). Increasing the applied force to about 200 pN changes the AFM topographs significantly because the prominent EF loops are bent away and the shorter loops of the BR monomers become visible (Fig. 5A, center-bottom and Fig. 5C). At elevated force, this nanomanipulation is fully reversible (Müller et al., 1995a) suggesting that loop EF is a rather flexible element on the cytoplasmic surface of the BR molecule. The maximum height difference between the protein and the lipid membrane is 0.6 ± 0.1 nm. Four distinct protrusions can be recognized in almost every monomer and a further, smaller protrusion is present at the center of the trimers

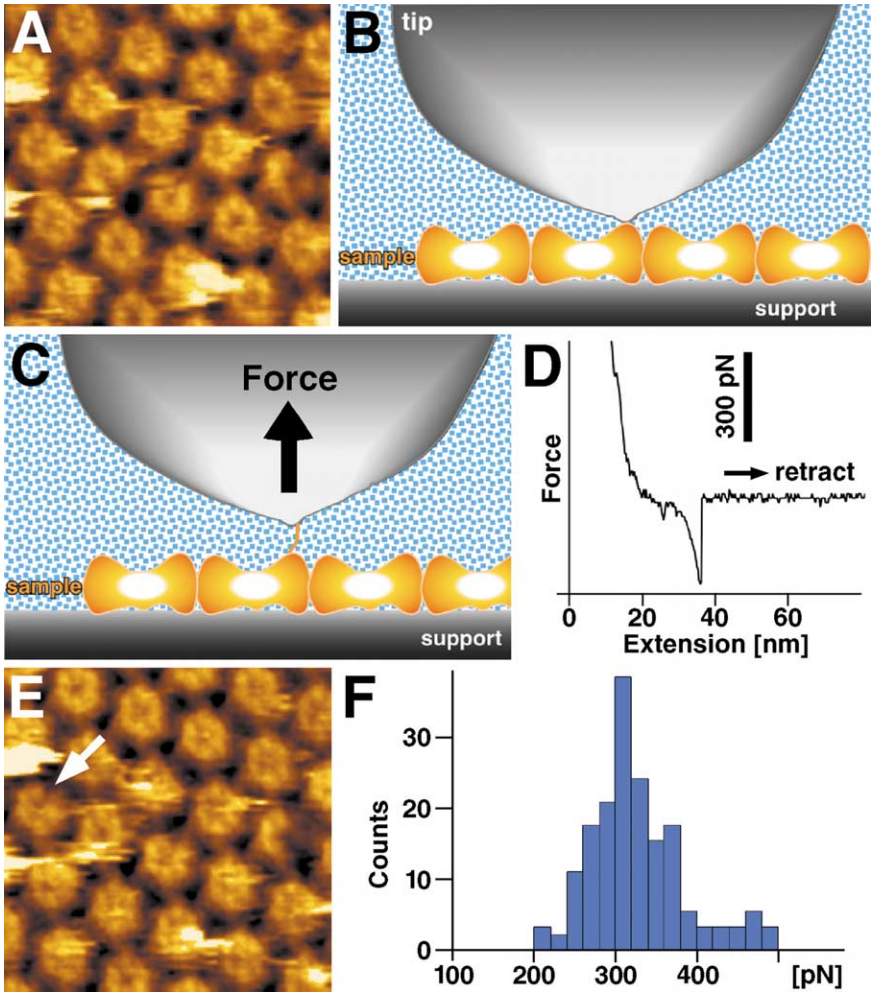

Fig. 6. Imaging and force spectroscopy of single protomers from a bacterial S-layer. (A) AFM topograph of the inner surface of the regular bacterial S-layer (HPI-layer) from the archaebacterium *Deinoccocus radiodurans*. (B) After recording the topograph, the AFM probe was pushed onto the bacterial surface for about 1 s at an applied force of ~1 nN. In about 25% of all approaches the N-terminal end of a protomer adsorbed to the AFM probe. (C) With this molecular bridge the AFM probe was then retracted and the cantilever deflection recorded. (D) Occasionally, the resulting force-extension curve showed a single adhesion peak of ~300 pN. (E) The same surface area imaged after recording the force-extension curve showed that a single protomer had been torn out of the layer (white arrow). (F) Histogram of adhesion forces measured upon the removal of single protomers. The Gaussian distribution of 198 measurements centers at 312 ± 43 pN. The hexamer-to-hexamer distance is 18 nm. Contact mode topographs were recorded in buffer solution (150 mM KCl, 20 mM $MgCl_2$, 10 mM Tris–HCl, pH 7.8) and exhibit a vertical brightness range of 3 nm.

(Fig. 5C). The calculated diffraction pattern of the topograph in Fig. 5A documents an isotropic resolution out to 0.5 nm (Müller et al., 1999c).

At an imaging force of 200 pN, the standard deviation of the height measurements made was around 0.1 nm for most morphological features of the topography while the EF loop exhibited a standard deviation of 0.2 nm (Fig. 5C, red shaded inset) reflecting its high flexibility (Müller et al., 1999c). This is consistent with the high temperature factors observed in the models from electron crystallography (Grigorieff et al., 1996; Mitsuoka et al., 1999) and the structural variation among the atomic BR models from X-ray crystallography (Heymann et al., 1999). The observed EF loop flexibility of BR is important for the efficient transport of protons across the bacterial membrane (Brown et al., 1995).

Similar to the above results, the reversible force-induced modulation of flexible protein domains has been observed on the ϕ29 phage connector (Müller et al., 1997b) and on aquaporin-Z from *Escherichia coli* (Scheuring et al., 1999). The flexibility of the ϕ29 connector ends are important for the ATP driven rotation of this connector implicated in the translocation of DNA into the phage capsid (Simpson et al., 2000).

8. Single molecule imaging and assessment of intermolecular forces

Structural, chemical and morphological studies have shown that the S-layers of bacteria are one of the most simple membrane structures developed during evolution (Baumeister et al., 1988). They completely cover the cell

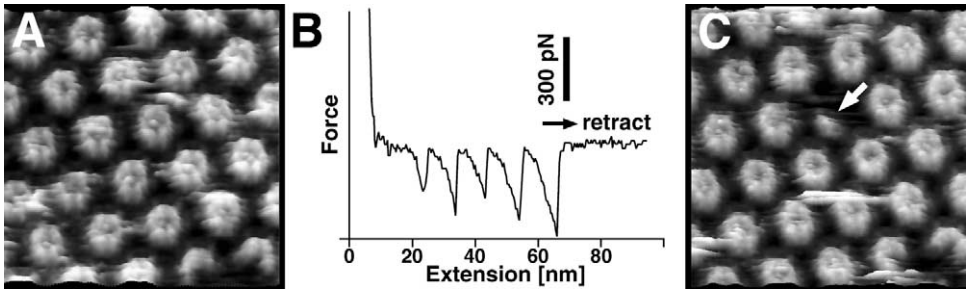

Fig. 7. Unzipping a hexameric bacterial S-layer protein into several protomers. (A) Inner surface of the S-layer (HPI-layer) of the archaebacterium *Deinoccocus radiodurans*. The six protomers forming each complex can be clearly distinguished. (B) The force-extension curve recorded from this surface shows a saw tooth pattern with five equally spaced peaks of ~300 pN separated by ~7 nm. (C) Same surface area imaged after recording the force-extension curve. As clearly seen from the molecular defect (white arrow), five protomers were removed. The hexamer-to-hexamer distance is 18 nm. Contact mode topographs (A and C) were recorded in buffer solution (150 mM KCl, 20 mM $MgCl_2$, 10 mM Tris–HCl, pH 7.8), exhibit a vertical full gray level range of 3 nm and are displayed as reliefs tilted by 5°.

surface and are usually composed of a single protein that is endowed with the ability to assemble into highly ordered monomolecular arrays by an entropy driven process (Sleytr et al., 1993). Experimental results indicate that the integrity of the S-layer lattice is maintained by different combinations of weak bonds which together are stronger than the bonds binding the S-layer to the underlying cell envelope (Sleytr et al., 1993; Sleytr, 1997).

The inner surface of the S-layer from the archaebacterium *Deinoccocus radiodurans*, the hexagonally packed intermediate (HPI)-layer, is anchored to the underlying outer cell membrane via strong hydrophobic interactions of the N-terminus (Thompson et al., 1982). The marked hydrophobicity of the N-terminus is caused by covalently bound fatty acids (Peters et al., 1987). The C-terminal region which is located on the outer surface of the HPI-layer, is covalently linked to a ~40 nm thick carbohydrate coat (Baumeister et al., 1982). This carbohydrate moiety helps to attach the bacteria to favourable areas.

The force anchoring a single protomer in its hexameric assembly reflects the coupling of lattice interactions within the S-layer and adhesion forces to the cell body. Investigation of isolated HPI-layers adsorbed to mica has allowed the interaction forces between individual protomers to be determined. For this single molecule force spectroscopy, the inner surface of the HPI-layer was first imaged (Fig. 6A). The resolution of the topograph was sufficient to resolve the individual subunits of the hexamers and their emanating arms. Afterwards, the AFM probe was attached to an individual protomer by increasing the force (~1 nN) applied to the silicon nitride tip to enforce probe-sample contact (Fig. 6B) for approximately 1 s. The change in cantilever deflection on tip retraction was then monitored (Fig. 6C). As visible from the force-extension curve (Fig. 6D), there was resistance to probe retraction approximately 15 nm from the contact point. This indicates that a molecular structure bridged the gap between the AFM probe and the HPI-layer. The structure readily extended to a length of ~21 nm, after which the bridge ruptured. This molecular bridge was possibly formed by interaction of the hydrophobic N-terminus with the tip. Imaging the HPI-layer after recording force-extension curves allowed the adhesion forces measured to be correlated to structural alterations; a single protomer was missing from one HPI hexamer (Fig. 6E, white arrow). Pulling forces of 312 ± 43 pN allowed individual protomers of the HPI-layer to be removed at will (Fig. 6F).

Occasionally, multiple peaks were observed in the force-extension curves. Fig. 7B displays a curve which exhibits five major equally spaced peaks (200–300 pN), while the corresponding control topograph shows that during retraction of the AFM probe five subunits have been zipped out of the bacterial S-layer (Fig. 7C, white arrow; compare with Fig. 7A). The probability of pulling several protomers out with a single tip retraction decreased with each protomer removed. Consequently, the process of 'unzipping' an entire HPI hexamer by removing all six monomers was quite rare (Müller et al., 1999a).

The spacing between the force peaks (Fig. 7B) indicates a strong interaction between protomers through flexible connecting links that have a length of about 7 nm. The observed adhesion peaks are quite similar in shape and magnitude to those detected on unfolding immunoglobulin segments of native and recombinant titin (Rief et al., 1997; Fisher et al., 1999). The best fit of the worm-like chain equation to the force-extension curves from the HPI-layer was obtained for a persistence length of 0.4 nm (Müller et al., 1999a) which is close to the persistence length of other proteins unfolded by the AFM (Rief et al., 1997; Oesterhelt et al., 2000). This value is related to the backbone structure of the polypeptide chain.

9. Single molecule imaging and detection of inter- and intramolecular forces

Membrane proteins acquire their function through specific folding of their polypeptide chain and through specific

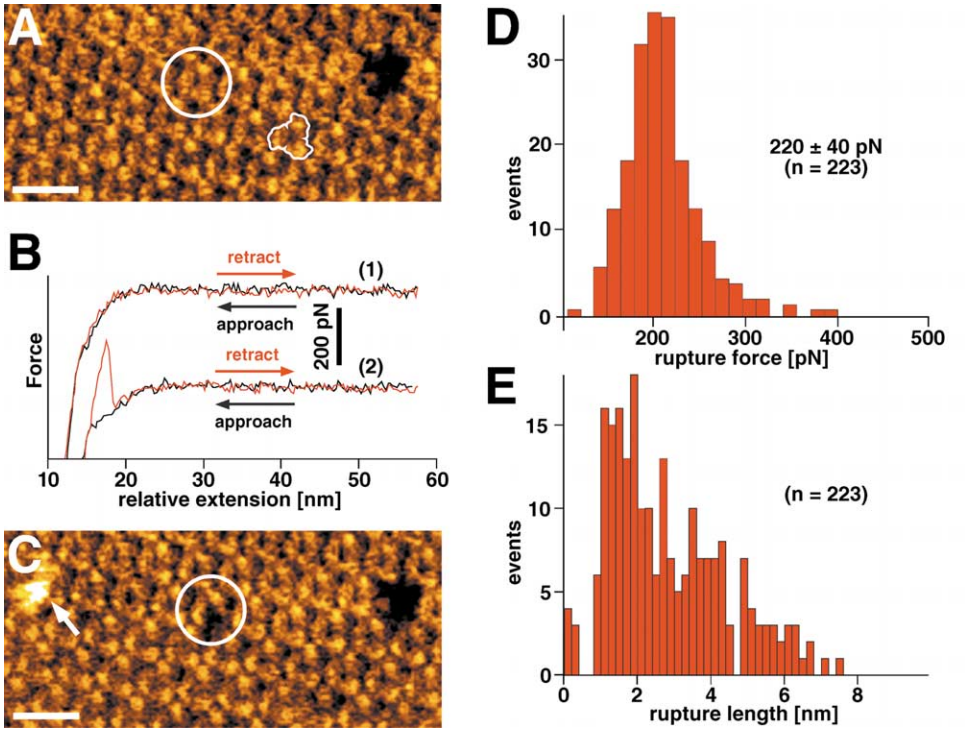

Fig. 8. Extracting individual bacteriorhodopsins from native purple membranes. (A) Topograph of the cytoplasmic side of purple membrane. BR trimers (outlined) are clearly visible. To attach an individual protein to the tip, the AFM probe was kept in contact with the membrane surface for about 1 s at an applied force of ~1 nN. (B) Most of the subsequent extension curves recorded on the cytoplasmic surface were unspectacular (1). However, 10% of the extension curves showed one adhesion peak (2). (C) The topograph of the same surface imaged after recording the force-extension curve (B, (2)): One BR monomer was missing (white circle). Immediately after this extraction a protrusion of about the size of an individual BR molecule was observed on the membrane surface (white arrow). The missing trimer at the upper right was used to align the topographs. (D) Histogram of the rupture forces required to extract an individual BR from the purple membrane. The average adhesion force was 220 ± 40 pN ($n = 223$). (E) Histogram of the rupture lengths measured to extract individual BRs from the membrane. The vertical brightness range of the topographs (A and C) is 1.5 nm. Topographs were recorded in buffer solution (300 mM KCl, 10 mM Tris–HCl, pH 7.8) using contact mode AFM.

interactions with the lipid bilayer and adjacent proteins. The stability and resistance of membrane proteins to unfolding is predominantly investigated by studying their thermal or chemical denaturation (Haltia and Freire, 1995; White and Wimley, 1999). Membrane proteins are designed to remain stable when embedded in lipid leaflets. Thus, their overall stability and resistance to denaturation depends on interactions with the hydrophobic core of the membrane (Haltia and Freire, 1995). As described by the fluid mosaic model (Singer and Nicolson, 1972) and the more recent raft model (Harder and Simons, 1997; Simons and Ikonen, 1997; Brown and London, 1998), a membrane protein together with a few tightly bound lipids can laterally diffuse within the bilayer, whereas vertically it is firmly anchored. Accordingly, it is of interest to directly measure the forces that anchor membrane proteins in the lipid bilayer. This can be done by combining AFM imaging and single molecule force spectroscopy.

Experiments performed with purple membrane provide a useful example. After imaging (Fig. 8A), the AFM probe was pushed towards the membrane surface with a loading force of about 1 nN. Force-extension curves were recorded as the tip was separated from the membrane surface (Fig. 8B). In 85% of the cases no adhesive force was observed (Fig. 8B, curve (1)). However, about 10% of the curves showed adhesive forces indicating that molecular structures had attached to the AFM probe and bridged the space in between (Fig. 8B, curve (2)). When the region was imaged again, an entire BR molecule was found to be missing (Fig. 8C, white circle). This implies that during retraction of the sample the BR molecule that had attached to the AFM probe was pulled out. Interestingly, the extracted BR molecule was frequently found adsorbed to the membrane surface close to its original position (Fig. 8C, white arrow). Repeating the experiment more than 200 times confirmed that such a single adhesion peak indeed reflects the extraction of an individual membrane protein and revealed its average adhesion force to be 220 ± 40 pN (Fig. 8D).

In most force-extension curves exhibiting a single peak (~95%), the adhesion force developed after the tip had been retracted by a short distance. The average extension occurring before the bond between the protein adsorbed to the AFM probe and the membrane broke was ~3 ± 2 nm (Fig. 8E). This length agrees favourably with the thickness of the hydrophobic region of the purple membrane bilayer (~3–3.5 nm) which anchors BR. This observation suggests

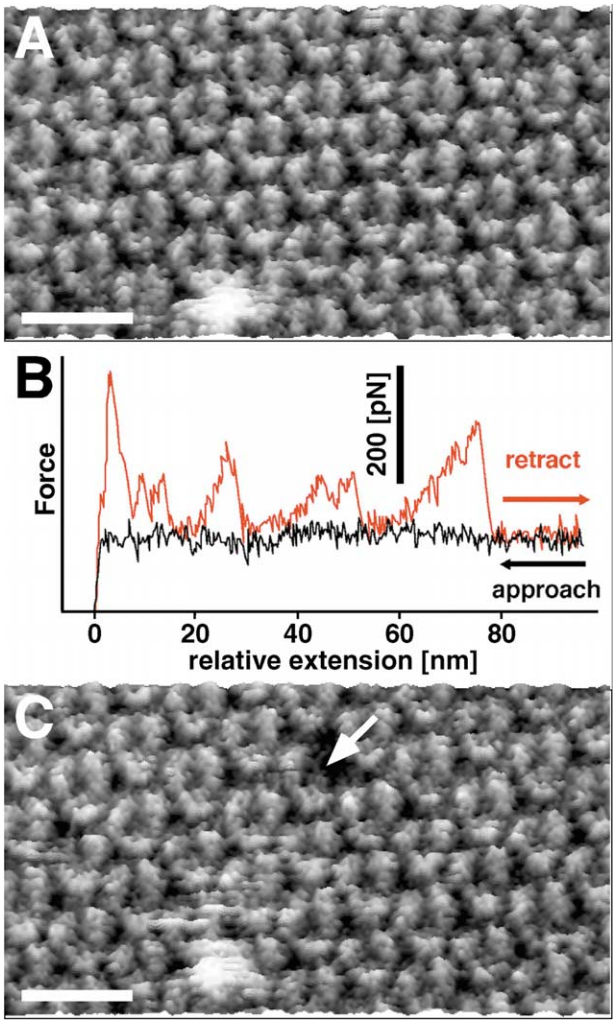

Fig. 9. Imaging and unfolding individual bacteriorhodopsins. (A) Topograph of the cytoplasmic purple membrane surface of wild type BR. (B) As described for Fig. 8, the AFM probe was pushed onto the membrane surface allowing a molecular bridge to be formed with BR. Force curves were subsequently recorded by retracting the probe from the purple membrane. The peaks in the force-extension curve extended far out to distances of ~75 nm corresponding to the length of one entirely unfolded BR protein (248 amino acids). (C) After acquisition of the force-extension curve, a topograph of the addressed surface area was recorded. The image clearly shows that one single BR monomer is missing. Topographs were recorded in buffer solution (300 mM KCl, 10 mM Tris–HCl, pH 7.8) using contact mode AFM. They exhibit a vertical full gray level range of 1.5 nm and were displayed as reliefs tilted by 5°.

that during such ruptures the entire BR molecule was extracted from the purple membrane in one single step (Oesterhelt et al., 2000).

In the experiments described above individual molecules were selected and addressed. Considering that the C-terminus of BR covers about one-quarter of the protein surface and consists of more than half of all amino acids accessible on the cytoplasmic side, the tip is likely to attach to the C-terminus. However, the precise attachment site is unknown. This uncertainty can be overcome by derivatizing the AFM tip and creating a specific link to the sample (Florin et al., 1994). For example, engineering a cysteine into the C-terminal region of BR (mutation at position G241C) has allowed the C-terminus to be covalently linked to a gold coated AFM probe (Oesterhelt et al., 2000). Most interestingly, the force-extension curves of BRs chemically anchored to the tip in this way were almost identical to those obtained from the wild type BR (Fig. 9). The molecular bridge formed in both cases extended to distances of ~75 nm. This corresponds to the length of an entirely unfolded BR. The analysis of the single molecule force curves and precise knowledge of the attachment site allowed the unfolding pathway to be predicted. Helices G and F as well as helices E and D always unfolded pairwise while helices B and C occasionally unfolded one after the other. Experiments with cleaved BR loops revealed the origin of this difference which is the result of both the stabilization of helix B by neighboring helices and the long loop connecting helices B and C (Oesterhelt et al., 2000).

10. Summary and outlook

The dissection of chromosomes and the controlled extraction of specific DNA segments are selected examples from the rapidly increasing number of experiments, where the AFM has been used for not only imaging biomolecules under native conditions, but also as a mechanical ‘scalpel’ and ‘shovel’. A refinement and extension of these applications will make the AFM a valuable tool for cytogenetic studies.

Imaging and manipulation of double-layered 2D crystals of membrane proteins has allowed the acquisition of valuable functional and structural information. Mechanical disruption of the upper layers of stacked crystalline sheets has enabled the investigation of otherwise hidden surfaces. It may also be possible to dissect living cells to expose and to explore their internal structure.

As demonstrated with photosystem I, the AFM probe can also be used to remove individual subunits from a protein complex. Single extrinsic proteins adhering to the reaction center have been imaged and then removed by the AFM stylus. After their removal, the underlying structure of the reaction center core could be imaged at high resolution. Thus, using the AFM a controlled dissection of supramolecular assemblies can be carried out and where feasible, previously hidden interfaces can be unveiled.

The controlled mechanical manipulation of selected molecules by force spectroscopy combined with high-resolution imaging is an extremely powerful approach to gain information on the molecular interactions occurring within biomolecular assemblies. Imaging before and after the force experiment may reveal whether the forces measured are of intra- or intermolecular nature. Initially designed as an imaging tool, the AFM has proved to be a multivalent instrument that allows single biomolecules to be

imaged, manipulated and dissected in a controlled manner. A wealth of novel information has emerged from such experiments within a few years. We expect future work with this versatile instrument to provide important insights into structure, dynamics and interactions of biomolecules in vitro and in vivo.

Acknowledgements

This work was supported by the M.E. Müller Foundation of Switzerland, by the Swiss National Foundation for Scientific research (Grant 4036-44062 to A.E.) and by the European Union-Biotech Program (Grant BIO4-CT98-0024 to A.E.). We thank Dr Stefan Thalhammer for kindly providing Fig. 1 and Dr Cora-Ann Schönenberger for critical reading of the manuscript.

References

Alexander, S., Hellemans, L., Marti, O., Schneir, J., Elings, V., Hansma, P.K., 1989. An atomic-resolution atomic-force microscope implemented using an optical lever. J. Appl. Phys. 65, 164–167.

Baumeister, W., Karrenberg, F., Rachel, R., Engel, A., ten Heggeler, B., Saxton, W.O., 1982. The major envelope protein of Micrococcus radiodurans (R1). Structural and chemical characterization. Eur. J. Biochem. 125, 535–544.

Baumeister, W., Wildhaber, I., Engelhardt, H., 1988. Bacterial surface proteins: Some structural, functional and evolutionary aspects. Biophys. Chem. 29, 39–49.

Benedetti, E.L., Dunia, I., Recouvreur, M., Nicolas, P., Kumar, N.M., Bloemendal, H., 2000. Structural organization of gap junctions as revealed by freeze-fracture and SDS fracture-labeling. Eur. J. Cell Biol. 79, 575–582.

Binnig, G., Quate, C.F., Gerber, C., 1986. Atomic force microscope. Phys. Rev. Lett. 56, 930–933.

Brown, D.A., London, E., 1998. Functions of lipid rafts in biological membranes. Annu. Rev. Cell. Dev. Biol. 14, 111–136.

Brown, L.S., Varo, G., Needleman, R., Lanyi, J.K., 1995. Functional significance of a protein conformation change at the cytoplasmic end of helix F during the bacteriorhodopsin photocycle. Biophys. J. 69, 2103–2111.

Cheung, C.L., Hafner, J.H., Lieber, C.M., 2000. Carbon nanotube atomic force microscopy tips: Direct growth by chemical vapor deposition and application to high-resolution imaging. Proc. Natl. Acad. Sci. USA. 97, 3809–3813.

Clausen-Schaumann, H., Seitz, M., Krautbauer, R., Gaub, H.E., 2000. Force spectroscopy with single bio-molecules. Curr. Opin. Chem. Biol. 4, 524–530.

Czajkowsky, D.M., Shao, Z., 1998. Submolecular resolution of single macromolecules with atomic force microscopy. FEBS Lett. 430, 51–54.

Czajkowsky, D.M., Sheng, S., Shao, Z., 1998. Staphylococcal alpha-hemolysin can form hexamers in phospholipid bilayers. J. Mol. Biol. 276, 325–330.

de Grooth, B.G., Putman, C.A., 1992. High-resolution imaging of chromosome-related structures by atomic force microscopy. J. Microsc. 168, 239–247.

Drake, B., Prater, C.B., Weisenhorn, A.L., Gould, S.A., Albrecht, T.R., Quate, C.F., Cannell, D.S., Hansma, H.G., Hansma, P.K., 1989. Imaging crystals, polymers and processes in water with the atomic force microscope. Science 243, 1586–1589.

Engel, A., Müller, D.J., 2000. Observing single biomolecules at work with the atomic force microscope. Nature Struct. Biol. 7, 715–718.

Engel, A., Schoenenberger, C.-A., Müller, D.J., 1997. High resolution imaging of native biological sample surfaces using scanning probe microscopy. Curr. Opin. Struct. Biol. 7, 279–284.

Fisher, T.E., Marszalek, P.E., Fernandez, J.M., 2000. Stretching single molecules into novel conformations using the atomic force microscope. Nature Struct. Biol. 7, 719–724.

Fisher, T.E., Oberhauser, A.F., Carrion-Vazquez, M., Marszalek, P.E., Fernandez, J.M., 1999. The study of protein mechanics with the atomic force microscope. Trends Biochem. Sci. 24, 379–384.

Florin, E.L., Moy, V.T., Gaub, H.E., 1994. Adhesion forces between individual ligand-receptor pairs. Science 264, 415–417.

Fotiadis, D., Hasler, L., Müller, D.J., Stahlberg, H., Kistler, J., Engel, A., 2000. Surface tongue-and-groove contours on lens MIP facilitate cell-to-cell adherence. J. Mol. Biol. 300, 779–789.

Fotiadis, D., Müller, D.J., Tsiotis, G., Hasler, L., Tittmann, P., Mini, T., Jenö, P., Gross, H., Engel, A., 1998. Surface analysis of the photosystem I complex by electron and atomic force microscopy. J. Mol. Biol. 283, 83–94.

Fritzsche, W., Henderson, E., 1996. Volume determination of human metaphase chromosomes by scanning force microscopy. Scanning Microsc. 10, 103–110.

Fritzsche, W., Schaper, A., Jovin, T.M., 1994. Probing chromatin with the scanning force microscope. Chromosoma. 103, 231–236.

Grandbois, M., Clausen-Schaumann, H., Gaub, H., 1998. Atomic force microscope imaging of phospholipid bilayer degradation by phospholipase A_2. Biophys. J. 74, 2398–2404.

Grigorieff, N., Ceska, T.A., Downing, K.H., Baldwin, J.M., Henderson, R., 1996. Electron-crystallographic refinement of the structure of bacteriorhodopsin. J. Mol. Biol. 259, 393–421.

Haltia, T., Freire, E., 1995. Forces and factors that contribute to the structural stability of membrane proteins. Biochim. Biophys. Acta. 1228, 1–27.

Han, W.H., Lindsay, S.M., Jing, T.W., 1996. A magnetically driven oscillating probe microscope for operation in liquids. Appl. Phys. Lett. 69, 4111–4113.

Han, W.H., Lindsay, S.M., Dlakic, M., Harrington, R.E., 1997. Kinked DNA. Nature 386, 563.

Hansma, H.G., Vesenka, J., Siegerist, C., Kelderman, G., Morrett, H., Sinsheimer, R.L., Elings, V., Bustamante, C., Hansma, P.K., 1992. Reproducible imaging and dissection of plasmid DNA under liquid with the atomic force microscope. Science 256, 1180–1184.

Hansma, P.K., Cleveland, J.P., Radmacher, M., Walters, D.A., Hillner, P.E., Bezanilla, M., Fritz, M., Vie, D., Hansma, H.G., Prater, C.B., Massie, J., Fukunaga, L., Gurley, J., Elings, V., 1994. Tapping mode atomic force microscopy in liquids. Appl. Phys. Lett. 64, 1738–1740.

Harder, T., Simons, K., 1997. Caveolae, DIGs and the dynamics of sphingolipid-cholesterol microdomains. Curr. Opin. Cell Biol. 9, 534–542.

Hasler, L., Walz, T., Tittmann, P., Gross, H., Kistler, J., Engel, A., 1998. Purified lens major intrinsic protein (MIP) forms highly ordered tetragonal two-dimensional arrays by reconstitution. J. Mol. Biol. 279, 855–864.

Henderson, E., 1992. Imaging and nanodissection of individual supercoiled plasmids by atomic force microscopy. Nucleic Acids Res. 20, 445–447.

Heymann, J.B., Müller, D.J., Landau, E.M., Rosenbusch, J.P., Pebay-Peyroula, E., Büldt, G., Engel, A., 1999. Charting the surfaces of the purple membrane. J. Struct. Biol. 128, 243–249.

Heymann, J.B., Pfeiffer, M., Hildebrandt, V., Kaback, H.R., Fotiadis, D., de Groot, B., Engel, A., Oesterhelt, D., Müller, D.J., 2000. Conformations of the rhodopsin third cytoplasmic loop grafted onto bacteriorhodopsin. Structure 8, 643–653.

Hillner, P.E., Walters, D.A., Lal, R., Hansma, H.G., Hansma, P.K., 1995. Combined atomic force and confocal laser scanning microscope. JMSA 1, 127–130.

Hoh, J.H., Lal, R., John, S.A., Revel, J.-P., Arnsdorf, M.F., 1991. Atomic

force microscopy and dissection of gap junctions. Science 253, 1405–1408.

Hoh, J.H., Sosinsky, G.E., Revel, J.-P., Hansma, P.K., 1993. Structure of the extracellular surface of the gap junction by atomic force microscopy. Biophys. J. 65, 149–163.

Humphris, A.D.L., Tamayo, J., Miles, M.J., 2000. Active quality factor control in liquids for force spectroscopy. Langmuir 16, 7891–7894.

Jondle, D.M., Ambrosio, L., Vesenka, J., Henderson, E., 1995. Imaging and manipulating chromosomes with the atomic force microscope. Chromosome Res. 3, 239–244.

Karrasch, S., Typke, D., Walz, T., Miller, M., Tsiotis, G., Engel, A., 1996. Highly ordered two-dimensional crystals of photosystem I reaction center from *Synechococcus* sp.: Functional and structural analyses. J. Mol. Biol. 262, 336–348.

Kasas, S., Thomson, N.H., Smith, B.L., Hansma, H.G., Zhu, X., Guthold, M., Bustamante, C., Kool, E.T., Kashlev, M., Hansma, P.K., 1997. *Escherichia coli* RNA polymerase activity observed using atomic force microscopy. Biochemistry 36, 461–468.

McMaster, T.J., Winfield, M.O., Baker, A.A., Karp, A., Miles, M.J., 1996a. Chromosome classification by atomic force microscopy volume measurement. J. Vac. Sci. Technol. B. 14, 1438–1443.

McMaster, T.J., Winfield, M.O., Karp, A., Miles, M.J., 1996b. Analysis of cereal chromosomes by atomic force microscopy. Genome 39, 439–444.

Meyer, G., Amer, N.M., 1988. Novel optical approach to atomic force microscopy. Appl. Phys. Lett. 53, 1045–1047.

Mitsuoka, K., Hirai, T., Murata, K., Miyazawa, A., Kidera, A., Kimura, Y., Fujiyoshi, Y., 1999. The structure of bacteriorhodopsin at 3.0 Å resolution based on electron crystallography: Implication of the charge distribution. J. Mol. Biol. 286, 861–882.

Möller, C., Allen, M., Elings, V., Engel, A., Müller, D.J., 1999. Tapping-mode atomic force microscopy produces faithful high-resolution images of protein surfaces. Biophys. J. 77, 1150–1158.

Mosher, C., Jondle, D., Ambrosio, L., Vesenka, J., Henderson, E., 1994. Microdissection and measurement of polytene chromosomes using the atomic force microscope. Scanning Microsc. 8, 491–497.

Mou, J., Sheng, S., Ho, R., Shao, Z., 1996. Chaperonins GroEL and GroES: Views from atomic force microscopy. Biophys. J. 71, 2213–2221.

Mou, J., Yang, J., Shao, Z., 1995. Atomic force microscopy of cholera toxin B-oligomers bound to bilayers of biologically relevant lipids. J. Mol. Biol. 248, 507–512.

Müller, D.J., Büldt, G., Engel, A., 1995a. Force-induced conformational change of bacteriorhodopsin. J. Mol. Biol. 249, 239–243.

Müller, D.J., Schabert, F.A., Büldt, G., Engel, A., 1995b. Imaging purple membranes in aqueous solutions at sub-nanometer resolution by atomic force microscopy. Biophys. J. 68, 1681–1686.

Müller, D.J., Baumeister, W., Engel, A., 1996a. Conformational change of the hexagonally packed intermediate layer of *Deinococcus radiodurans* imaged by atomic force microscopy. J. Bacteriol. 178, 3025–3030.

Müller, D.J., Schoenenberger, C.-A., Büldt, G., Engel, A., 1996b. Immuno-atomic force microscopy of purple membrane. Biophys. J. 70, 1796–1802.

Müller, D.J., Engel, A., Amrein, M., 1997a. Preparation techniques for the observation of native biological systems with the atomic force microscope. Biosens. Bioelect. 12, 867–877.

Müller, D.J., Engel, A., Carrascosa, J., Veléz, M., 1997b. The bacteriophage ϕ29 head-tail connector imaged at high resolution with the atomic force microscope in buffer solution. EMBO J. 16, 2547–2553.

Müller, D.J., Engel, A., 1999. Voltage and pH-induced channel closure of porin OmpF visualized by atomic force microscopy. J. Mol. Biol. 285, 1347–1351.

Müller, D.J., Baumeister, W., Engel, A., 1999a. Controlled unzipping of a bacterial surface layer with atomic force microscopy. Proc. Natl. Acad. Sci. USA. 96, 13170–13174.

Müller, D.J., Fotiadis, D., Scheuring, S., Müller, S.A., Engel, A., 1999b. Electrostatically balanced subnanometer imaging of biological specimens by atomic force microscope. Biophys. J. 76, 1101–1111.

Müller, D.J., Sass, H.-J., Müller, S.A., Büldt, G., Engel, A., 1999c. Surface structures of native bacteriorhodopsin depend on the molecular packing arrangement in the membrane. J. Mol. Biol. 285, 1903.

Nature Structural Biology, 2000. Special edition on: Monitoring molecular movements. Nature Struct. Biol. 7.

Oesterhelt, F., Oesterhelt, D., Pfeiffer, M., Engel, A., Gaub, H.E., Müller, D.J., 2000. Unfolding pathways of individual bacteriorhodopsins. Science 288, 143–146.

Perkins, G., Goodenough, D., Sosinsky, G., 1997. Three-dimensional structure of the gap junction connexon. Biophys. J. 72, 533–544.

Perkins, G., Goodenough, D., Sosinsky, G., 1998. Formation of the gap junction intercellular channel requires a 30° rotation for interdigitating two apposing connexons. J. Mol. Biol. 277, 171–177.

Peters, J., Peters, M., Lottspeich, F., Schäfer, W., Baumeister, W., 1987. Nucleotide sequence of the gene encoding the *Deinococcus radiodurans* surface protein, derived amino acid sequence, and complementary protein chemical studies. J. Bacteriol. 169, 5216–5223.

Putman, C.A.J., van Leeuwen, A.M., de Grooth, B.G., Radosevic, K., van der Werf, K., van Hulst, N.F., Greve, J., 1993. Atomic force microscopy combined with confocal laser scanning microscopy: A new look at cells. Bioimaging 1, 63–70.

Putman, C.A.J., Vanderwerf, K.O., de Grooth, B.G., Vanhulst, N.F., Greve, J., 1994. Tapping mode atomic-force microscopy in liquid. Appl. Phys. Lett. 64, 2454–2456.

Rasch, P., Wiedemann, U., Wienberg, J., Heckl, W.M., 1993. Analysis of banded human chromosomes and in situ hybridization patterns by scanning force microscopy. Proc. Natl. Acad. Sci. USA 90, 2509–2511.

Reviakine, I., Bergsma-Schutter, W., Brisson, A., 1998. Growth of protein 2-D crystals on supported planar lipid bilayers imaged in situ by AFM. J. Struct. Biol. 121, 356–361.

Rief, M., Gautel, M, Gaub, H.E., 2000. Unfolding forces of titin and fibronectin domains directly measured by AFM. Adv. Exp. Med. Biol. 481, 129–141.

Rief, M., Gautel, M., Oesterhelt, F., Fernandez, J.M., Gaub, H.E., 1997. Reversible unfolding of individual titin immunoglobulin domains by AFM. Science 276, 1109–1112.

Schabert, F., Knapp, H., Karrasch, S., Häring, R., Engel, A., 1994. Confocal scanning laser—scanning probe hybrid microscope for biological applications. Ultramicroscopy 53, 147–157.

Schabert, F.A., Engel, A., 1994. Reproducible acquisition of *Escherichia coli* porin surface topographs by atomic force microscopy. Biophys. J. 67, 2394–2403.

Schabert, F.A., Henn, C., Engel, A., 1995. Native *Escherichia coli* OmpF porin surfaces probed by atomic force microscopy. Science 268, 92–94.

Scheuring, S., Ringler, P., Borgina, M., Stahlberg, H., Müller, D.J., Agre, P., Engel, A., 1999. High resolution AFM topographs of the *Escherichia coli* water channel aquaporin Z. EMBO J. 18, 4981–4987.

Schmitt, L., Ludwig, M., Gaub, H.E., Tampe, R., 2000. A metal-chelating microscopy tip as a new toolbox for single-molecule experiments by atomic force microscopy. Biophys. J. 78, 3275–3285.

Schoenenberger, C.-A., Hoh, J.H., 1994. Slow cellular dynamics in MDCK and R5 cells monitored by time-lapse atomic force microscopy. Biophys. J. 67, 929–936.

Schoenenberger, C.A., Müller, D.J., Engel, A., 1997. Atomic force microscopy provides molecular details of cell surfaces. In: Isenberg, G. (Ed.), Modern Optics, Electronics and High Precision Techniques in Cell Biology. Springer Verlag, Heidelberg, pp. 1–33.

Schubert, W.-D., Klukas, O., Krauss, N., Saenger, W., Fromme, P., Witt, H.T., 1997. Photosystem I of *Synechococcus elongatus* at 4 Å resolution: Comprehensive structure analysis. J. Mol. Biol. 272, 741–769.

Science. 1999. Special edition on: Frontiers in chemistry—single molecules. Science, 283.

Shao, Z., Yang, J., 1995. Progress in high resolution atomic force microscopy in biology. Q. Rev. Biophys. 28, 195–251.

Shiels, A., Bassnett, S., 1996. Mutations in the founder of the MIP gene

family underlie cataract development in the mouse. Nature Genet. 12, 212–215.
Shiels, A., Mackay, D., Bassnett, S., Al-Ghoul, K., Kuszak, J., 2000. Disruption of lens fiber cell architecture in mice expressing a chimeric AQP0-LTR protein. FASEB J. 14, 2207–2212.
Simons, K., Ikonen, E., 1997. Functional rafts in cell membranes. Nature 387, 569–572.
Simpson, A.A., Tao, Y., Leiman, P.G., Badasso, M.O., He, Y., Jardine, P.J., Olson, N.H., Morais, M.C., Grimes, S., Anderson, D.L., Baker, T.S., Rossmann, M.G., 2000. Structure of the bacteriophage phi29 DNA packaging motor. Nature 408, 745–750.
Singer, S.J., Nicolson, G.L., 1972. The fluid mosaic model of the structure of cell membranes. Science 175, 720–731.
Sleytr, U.B., 1997. Basic and applied S-layer research: An overview. FEMS Microbiol. Rev. 20, 5–12.
Sleytr, U.B., Messner, P., Pum, D., Sara, M., 1993. Crystalline bacterial cell surface layers. Mol. Microbiol. 10, 911–916.
Sosinsky, G.E., 1996. Molecular organization of gap junction membrane channels. J. Bioenerg. Biomembr. 28, 297–309.
Stark, R.W., Thalhammer, S., Wienberg, J., Heckl, W.M., 1998. The AFM as a tool for chromosomal dissection—the influence of physical parameters. Appl. Phys. A. 66, S579–S584.
Tamayo, J., Garcia, R., 1996. Deformation, contact time and phase contrast in tapping mode scanning force microscopy. Langmuir 12, 4430–4435.
Thalhammer, S., Stark, R.W., Müller, S., Wienberg, J., Heckl, W.M., 1997. The atomic force microscope as a new microdissecting tool for the generation of genetic probes. J. Struct. Biol. 119, 232–237.
Thompson, B.G., Murray, R.G.E., Boyce, J.F., 1982. The association of the surface array and the outer membrane of *Deinococcus radiodurans*. Can. J. Microbiol. 28, 1081–1088.
Unger, V.M., Kumar, N.M., Gilula, N.B., Yeager, M., 1999. Three-dimensional structure of recombinant gap junction membrane channel. Science 283, 1176–1180.
Unwin, P.N., Ennis, P.D., 1984. Two configurations of a channel-forming membrane protein. Nature 307, 609–613.
Vesenka, J., Guthold, M., Tang, C.L., Keller, D., Delaine, E., Bustamante, C., 1992. Substrate preparation for reliable imaging of DNA molecules with the scanning force microscope. Ultramicroscopy 42-44, 1243–1249.
Vesenka, J., Mosher, C., Schaus, S., Ambrosio, L., Henderson, E., 1995. Combining optical and atomic force microscopy for life sciences research. Biotechniques 19, 240–248.
Viani, M.B., Pietrasanta, L.I., Thompson, J.B., Chand, A., Gebeshuber, I.C., Kindt, J.H., Richter, M., Hansma, H.G., Hansma, P.K., 2000. Probing protein–protein interactions in real time. Nature Struct. Biol. 7, 644–647.
Viani, M.B., Schäfer, T.E., Chand, A., Rief, M., Gaub, H.E., Hansma, P.K., 1999. Small cantilevers for force spectroscopy of single molecules. J. Appl. Phys. 86, 2258–2262.
Wagner, P., 1998. Immobilization strategies for biological scanning probe microscopy. FEBS Lett. 430, 112–115.
Walters, D.A., Cleveland, J.P., Thomson, N.H., Hansma, P.K., Wendman, M.A., Gurley, G., Elings, V., 1996. Short cantilevers for atomic force microscopy. Rev. Sci. Instrum. 67, 3583–3590.
Walz, T., Tittmann, P., Fuchs, K.H., Müller, D.J., Smith, B.L., Agre, P., Gross, H., Engel, A., 1996. Surface topographies at subnanometer-resolution reveal asymmetry and sidedness of aquaporin-1. J. Mol. Biol. 264, 907–918.
Weisenhorn, A.L., Hansma, P.K., Albrecht, T.R., Quate, C.F., 1989. Forces in atomic force microscopy in air and water. Appl. Phys. Lett. 54, 2651–2653.
White, S.H., Wimley, W.C., 1999. Membrane protein folding and stability: Physical principles. Annu. Rev. Biophys. Biomol. Struct. 28, 319–365.
Winfield, M., McMaster, T.J., Karp, A., Miles, M.J., 1995. Atomic force microscopy of plant chromosomes. Chromosome Res. 3, 128–131.
Xu, X.M., Ikai, A., 1998. Retrieval and amplification of single-copy genomic DNA from a nanometer region of chromosomes: A new and potential application of atomic force microscopy in genomic research. Biochem. Biophys. Res. Commun. 248, 744–748.
Zhong, Q., Inniss, D., Kjoller, K., Elings, V.B., 1993. Fractured polymer/silica fiber surface studied by tapping mode atomic force microscopy. Surf. Sci. Lett. 290, L688–L692.